

Pressure induced transformation and subsequent amorphization of monoclinic Nb₂O₅ and its effect on optical properties

Zhou Guan¹, Quanjun Li^{1,2}, Huafang Zhang¹, Pengfei Shen¹, Lirong Zheng³, Shengqi Chu³, Changyong Park², Xinguo Hong⁴, Ran Liu¹, Peng Wang¹, Bingbing Liu¹ and Guoyin Shen^{2,5}

¹ State Key Laboratory of Superhard Materials, Jilin University, Changchun 130012, People's Republic of China

² High Pressure Collaborative Access Team (HPCAT), Geophysical Laboratory, Carnegie Institute of Washington, Argonne, IL 60439, United States of America

³ Beijing Synchrotron Radiation Facility, Institute of High Energy Physics, Chinese Academy of Sciences, Beijing 100049, People's Republic of China

⁴ Center for High Pressure Science and Technology Advanced Research, Beijing 100094, People's Republic of China

⁵ X-ray Science Division, Argonne National Laboratory, Argonne, IL 60439, United States of America

E-mail: liquanjun@jlu.edu.cn and liubb@jlu.edu.cn

Received 9 July 2018, revised 11 December 2018

Accepted for publication 19 December 2018

Published 18 January 2019



Abstract

Pressure-induced phase transitions of monoclinic H-Nb₂O₅ have been studied by *in situ* synchrotron x-ray diffraction, pair distribution function (PDF) analysis, and Raman and optical transmission spectroscopy. The initial monoclinic phase is found to transform into an orthorhombic phase at ~9 GPa and then change to an amorphous form above 21.4 GPa. The PDF data reveal that the amorphization is associated with disruptions of the long-range order of the NbO₆ octahedra and the NbO₇ pentagonal bipyramids, whereas the local edge-shares of octahedra and the local linkages of pentagonal bipyramids are largely preserved in their nearest neighbors. Upon compression, the transmittance of the sample in a region from visible to near infrared (450–1000 nm) starts to increase above 8.0 GPa and displays a dramatic enhancement above 22.2 GPa, indicating that the amorphous form has a high transmittance. The pressure-induced amorphous form is found to be recoverable under pressure release, and maintain high optical transmittance property at ambient conditions. The recoverable pressure induced amorphous material promises for applications in multifunctional materials.

Keywords: Nb₂O₅, high-pressure, phase transitions, amorphization, transmittance

 Supplementary material for this article is available [online](#)

(Some figures may appear in colour only in the online journal)

1. Introduction

A pressure-induced amorphous form is intimately associated with its crystalline parent phase [1–3], displaying features that may be different from a traditional amorphous phase, such as retaining microclusters related to its crystalline parent [4]. The process of pressure-induced amorphization (PIA) has become

a powerful way for synthesis of new amorphous materials with novel properties [5–7]. Since the first observation in ice-H₂O [1], PIA has subsequently been observed in a number of tetrahedrally coordinated materials such as Si [2, 8, 9] and SiO₂ [10, 11], several octahedrally coordinated materials such as TiO₂ [12, 13] and Y₂O₃ [14], and in materials with complicated polyhedra such as V₂O₅ [15], Ta₂O₅ [16] and Nb₂O₅

[17–20]. The scientific research has never ceased from the initial tetrahedrally coordinated to octahedrally coordinated to complicated polyhedra. In recent years, PIA have also been reported in some other materials, such as perovskite [21–23], $(\text{Mg,Fe})_2\text{SiO}_4$ olivine [24] and tungstate [25], which are important for scientific and technological applications. Despite the wide observations in various materials, the structural relations to their parent crystalline phases remain unclear.

Nb_2O_5 has various applications in special optical glasses, chemical fiber panels, monolithic capacitors and piezoelectric ceramic elements because of its high dielectric constant, high refractive index, outstanding photoelectric properties, and high chemical stability [26–30]. This material is known to display several different polymorphs depending on pressure-temperature conditions to which this compound is subjected. The most commonly observed phases are as follows: H (P2/m, monoclinic), B (C2/c, monoclinic), N (C2/m, monoclinic), R (C2/m, monoclinic), M (I4/mmm, tetragonal), P (I4₁22, tetragonal), T (Pbam, orthorhombic), and TT (monoclinic or pseudo-hexagonal) [31–33]. In most Nb_2O_5 polymorphs, Nb is in octahedral oxygen coordination (NbO_6), except for the T- and TT-phases, where a fraction of Nb atoms are in sevenfold coordination (NbO_7) and eightfold hexagonal bipyramid (NbO_8) [33]. Thus, Nb_2O_5 is an appropriate case to study the underlying mechanism of PIA for a complicated system with various polyhedra. Recently, Kikuchi *et al* [17, 18] studied the phase transition of Nb_2O_5 under shock compression, and found that a transition from H- Nb_2O_5 to T- Nb_2O_5 occurs at a shock pressure of ~20 GPa, with the T- Nb_2O_5 further decomposing to a form of NbO_2 via an intermediate step at a shock pressure of ~40 GPa. However, Serghiou *et al* [19] observed PIA in T- Nb_2O_5 and proposed that the PIA is accompanied by a reduction of pentavalent Nb with the loss of oxygen atoms. Subsequently, x-ray photoelectron and x-ray absorption spectroscopy measurements showed there is no such pressure-induced reduction in T- Nb_2O_5 [20]. To date, the nature of the structural phase transition and PIA in Nb_2O_5 has been complicated and unclear. In addition, there is still no experimental report about the definite PIA mechanism and property for the H- Nb_2O_5 phase under the condition of hydrostatic pressure. This work aims to provide insights into the understanding PIA mechanisms of H- Nb_2O_5 and explore pressure-induced amorphous materials with novel properties.

In this study, we have investigated the phase transitions in monoclinic H- Nb_2O_5 using *in situ* synchrotron x-ray diffraction (XRD), pair distribution function (PDF) analysis, and Raman and optical transmission spectroscopies. The monoclinic phase is found to transform into an orthorhombic phase at ~9 GPa and then change to an amorphous form above 21.4 GPa. The PIA mechanism for Nb_2O_5 is associated with the breakdown of the long-range order of the polyhedra (NbO_6 octahedra and NbO_7 pentagonal bipyramids). Moreover, the transmission spectra reveal an order of magnitude increase in the transmittance of pressure-induced amorphous Nb_2O_5 , a dramatic enhancement likely linked to the structural characteristics of the amorphous material via the PIA.

2. Experimental

The Nb_2O_5 (99.9985% purity) powder used in the experiment was obtained from Alfa Aesar. High-pressure experiments were generated by using a symmetric diamond-anvil cell (DAC) with a pair of diamonds of culet size of 400 μm . A stainless-steel gasket with a 130 μm hole was used as the sample chamber. The sample and a small ruby ball were loaded in the chamber with silicone oil (Dow Corning PMX-200 silicone fluid with a viscosity of 10 cst at 25 °C) for XRD or a 4:1 methanol-ethanol mixture for Raman and PDF as the pressure-transmitting medium. The hydrostatic limits for the 4:1 methanol-ethanol mixture and silicone oil are ~10.5 and ~3 GPa, respectively [34]. In optical transmission measurements, no pressure-transmitting medium was used. *In situ* angle-dispersive synchrotron XRD measurements under high pressure were carried out at the X17C beamline of the National Synchrotron Light Source (NSLS) at Brookhaven National Laboratory (BNL) and the 4W2 beamline of the Beijing Synchrotron Radiation Facility (BSRF), with the incident beam wavelengths of 0.4112 Å and 0.6199 Å, respectively. Some of the XRD experiments were carried out at the 16-BM-D beamline of the High Pressure Collaborative Access Team (HPCAT) at the Advanced Photon Source (APS), Argonne National Laboratory (ANL). Raman measurements were conducted using a LabRAM HR Evolution Raman spectrometer with 532 nm laser excitation. Data suitable for PDF analysis were collected at the 17B3 beamline of the NSLS, BNL. The high-pressure XAS measurements at the Nb K-edge (~18986 eV) were performed at the 1W2B beamline of the BSRF. The sample and amorphous boron powder (as the pressure medium) were mixed and sealed inside the DAC. The pressure was determined using ruby fluorescence techniques [35]. Both the starting and quenched samples were characterized by using transmission electron microscopy (TEM) (200 KV, Hitachi, H-8100IV), and high-resolution transmission electron microscopy (HRTEM) (JEOL JEM-3010). The optical transmission spectra were collected with a Bruker Vertex 80v UV–visible spectrometer. The diffraction data were recorded on an MAR345 imaging plate, and then the 2D Debye–Scherrer diffraction patterns were integrated into 1D data by using the Fit2D program. The XRD patterns were refined by using the GSAS software package with the Le Bail method [36]. PDF patterns were obtained by the program PDFgetX2 [37]. Background, Compton scattering, and absorption corrections were applied to the raw scattering data.

3. Results and discussion

3.1. XRD patterns at high pressures

Figure 1(a) shows the XRD patterns of Nb_2O_5 at selected pressures. All the observed diffraction peaks can be indexed with the monoclinic H- Nb_2O_5 phase below 4.7 GPa, shown in figure 1(b). With increasing pressure, the diffraction peaks are shifted to larger angles, indicating a pressure-induced reduction of d-spacing or shrinkage of the unit cells. Upon further compression to 5.9 GPa, several new peaks appear, indicating a transition to another phase. At 9.9 GPa, all the peaks of the

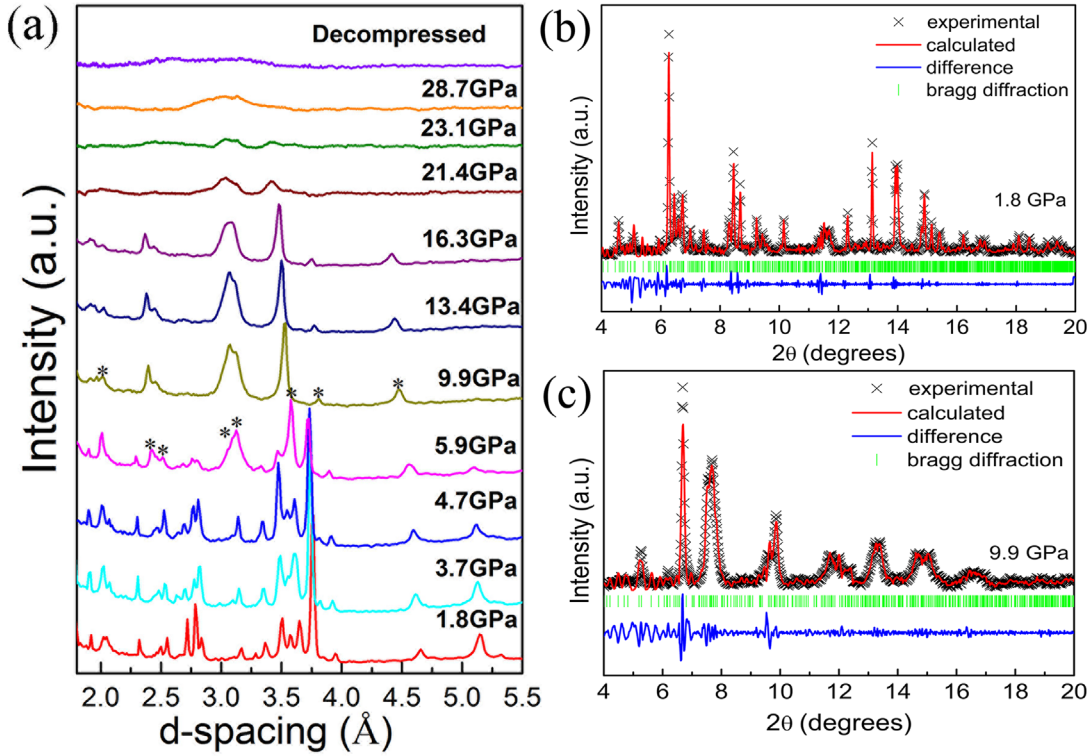


Figure 1. (a) XRD patterns of Nb₂O₅ obtained during compression and decompression. XRD patterns and their refinements for the Nb₂O₅ with (b) monoclinic and (c) orthorhombic phases. Diffraction peaks marked ‘*’ originate from the orthorhombic phase.

Table 1. Parameters for the monoclinic (M) phase at 1.8 GPa and the orthorhombic (O) phase at 9.9 GPa.

P (GPa)	Phase	<i>a</i> (Å)	<i>b</i> (Å)	<i>c</i> (Å)	<i>V</i> (Å ³)	<i>β</i> (°)	Rwp (%)	Rp (%)	χ ² (%)
1.8	M	21.228(2)	3.835(1)	19.413(2)	1366.49 (19)	119.87(1)	0.89	0.52	3.71
9.9	O	6.176 (1)	39.915 (11)	3.929(1)	968.67 (30)		0.69	0.40	2.41

monoclinic H-Nb₂O₅ phase disappear [38–40]. The peaks of the high-pressure phase above 9.9 GPa can be indexed with an orthorhombic structure similar to the orthorhombic L-Ta₂O₅ phase (space group P_{2mm}) [41–43]. This high pressure orthorhombic phase is different from the T-Nb₂O₅ (space group Pbam) [32]. Figure 1(c) shows the results of the refinement assuming the orthorhombic L-Ta₂O₅ structure for the high-pressure phase. Table 1 lists the refined parameters for the monoclinic (1.8 GPa) and orthorhombic (9.9 GPa) phases. With further increasing pressure, most diffraction peaks disappear at 21.4 GPa, except the two broad bands at approximately 3.0 Å and 3.4 Å, which are associated with an amorphous phase [44, 45]. Subsequently, the two broad bands are further broadened and weakened with increasing pressure, yet still detectable up to a pressure of 28.7 GPa. Upon decompression, the amorphous phase is retained at ambient pressure, indicating its recoverability under decompression. In our case, the transition from H-Nb₂O₅ to the orthorhombic L-Ta₂O₅-like phase is different from the early reported H-Nb₂O₅-to-T-Nb₂O₅ transition induced by shock compression [17, 18]. Moreover, the PIA of H-Nb₂O₅ undergoes an intermediate orthorhombic phase, which is also different from those direct amorphization from the starting phase under high pressure that observed in TiO₂ [12], Y₂O₃ [14], Ta₂O₅ [16], and T-Nb₂O₅ [19].

Figure 2(a) shows the unit cell parameters of the monoclinic phase as a function of pressure. Obviously, the pressure dependences of the unit cell parameters of *a*, *b*, and *c* are different in the pressure range of 1.8–4.7 GPa. The different compressibilities along *a*, *b* and *c* axes indicate the anisotropic properties of the monoclinic phase. The pressure-volume data of the monoclinic phase is shown in figure 2(b). The pressure-volume data were fitted to the Birch–Murnaghan equation of state:

$$P = \frac{3B_0}{2} \left[\left(\frac{V}{V_0} \right)^{-\frac{2}{3}} - \left(\frac{V}{V_0} \right)^{-\frac{5}{3}} \right] \times \left\{ 1 + \frac{3}{4} (B_0' - 4) \left[\left(\frac{V}{V_0} \right)^{-\frac{2}{3}} - 1 \right] \right\} \quad (1)$$

where *B*₀ and *B*'₀ are the isothermal bulk modulus and its pressure derivative, respectively, and *V*₀ is the unit-cell volume at ambient pressure. The bulk modulus (*B*₀) of the monoclinic phase is determined to be 132(4) GPa, with *B*'₀ fixed at 4. It is some lower than the calculated result of 158 GPa [33].

3.2. Raman spectra at high pressures

To further verify the pressure-induced phase transition of Nb₂O₅, we also conducted *in situ* high-pressure Raman spectra measurements, as shown in figure 3(a). From the group

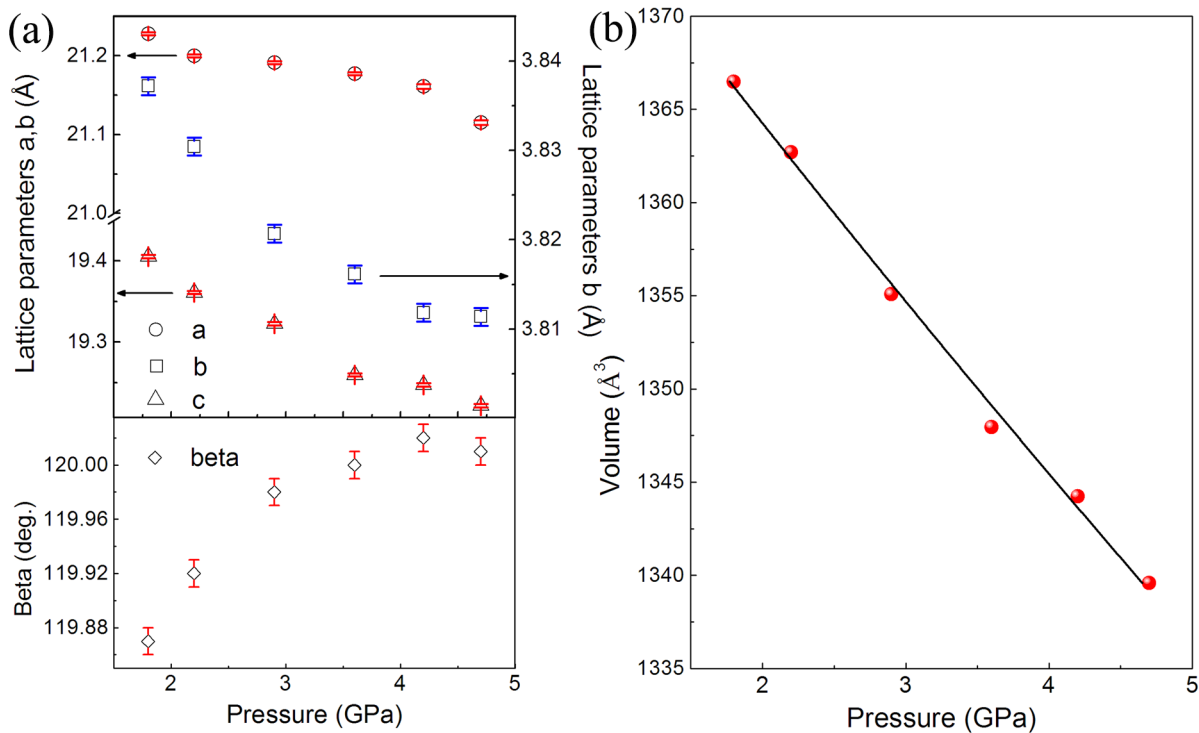


Figure 2. (a) Variation in relative lattice parameters (a , b , c , and β) of H-Nb₂O₅ with pressure. (b) Pressure-volume diagram of H-Nb₂O₅.

analysis, there are 154 Raman active modes: 95 A_g and 49 B_g . At ambient conditions, the Raman spectra of H-Nb₂O₅, shown in figure 3(b), bottom), exhibit several peaks of the lattice vibrations including one sharp peak at 992 cm⁻¹ and several broad peaks at 112, 122, 230, 257, 299, 622, and 649 cm⁻¹ [46, 47]. The Raman peaks between 180 and 350 cm⁻¹ are the group characteristic of the Nb–O–Nb angle deformation. Those peaks between 380 and 520 cm⁻¹ correspond to the O–Nb₃ structure. The peaks between 580 and 740 cm⁻¹ are assigned to the Nb–O–Nb bridging bond that leads to the anisotropy of the NO₆ octahedra. The peaks at 800–900 cm⁻¹ are caused by corner-sharing NbO₆ octahedra units. The sharp peak at 992 cm⁻¹ is attributed to edge-sharing NbO₆ octahedra units. The peaks below 180 cm⁻¹ are attributed to metal cation-cation bonds. With increasing pressure, all Raman peaks exhibit blue shifts, and their intensities weaken gradually. Figure 3(b), middle) shows the disappearance of the most characteristic peaks for H-Nb₂O₅ above ~8 GPa, such as those at 893, 834, 649, 622, 545 and 464 cm⁻¹; However, Raman peaks at 241, 688 and 1018 cm⁻¹ are still present. The peaks at 649 and 622 cm⁻¹ are merged into the peak at ~688 cm⁻¹. The peak at 1018 cm⁻¹ is caused by edge-sharing polyhedra, indicating edge-sharing polyhedra still remained. The Raman peaks between 100 and 450 cm⁻¹ in such oxide compounds generally correspond to O–Nb–O bending vibrations in the NbO₆ octahedra. Pure skeletal modes involving Nb–O–Nb bending coordinates in different types of polyhedra might contribute to several of these bending modes [48, 49]. As the pressure increased to 21.6 GPa, shown in figure 3(b), top), the Raman peaks disappear except the broad one at 690 cm⁻¹, which is consistent with the XRD data of the amorphous form [46]. The Raman bands are associated with the density of states of the amorphous phase [50]. In

addition, the broad Raman peak at ~690 cm⁻¹ is retained in the quenched sample at ambient conditions, in agreement with the XRD data showing that the PIA is irreversible in Nb₂O₅.

3.3. HRTEM and selected area electron diffraction (SAED)

To reveal the amorphous character of the recovered Nb₂O₅ from high pressure, we carried out TEM, HRTEM and SAED pattern analysis of both the initial sample and the sample decompressed from 31.1 GPa. As shown in figure S2(a) (stacks.iop.org/JPhysCM/31/105401/mmedia), the initial sample consists of irregular particles with sizes ranging from 0.8–2.8 μm. The HRTEM image, shown in figure 4(a), exhibits clear lattice fringes with the lattice spacings of 3.65 Å and 4.17 Å corresponding to ($\bar{1}05$) and ($\bar{5}03$) planes of monoclinic H-Nb₂O₅ (PDF 72-1121), respectively, indicating that the starting material has a good crystalline monoclinic structure. Figure S2(b) shows the TEM image of the amorphous Nb₂O₅ recovered from 31.1 GPa. As shown in figure 4(c), no lattice fringes are observed in the corresponding HRTEM image, demonstrating a totally disordered structure of the recovered sample. Figure 4(d) shows no clear and distinct diffraction rings, which further confirms that no long-range ordered structure exists in the recovered sample.

3.4. PDFs at high pressures

It is known that the monoclinic lattice of H-Nb₂O₅ contains $3 \times 4 \times \infty$ and $3 \times 5 \times \infty$ blocks comprising NbO₆ octahedra, in which each Nb atom is surrounded by six O atoms (the black boxes in figure 5(a)). These blocks are interconnected by edge-sharing (sharing two oxygen atoms) with a shift of

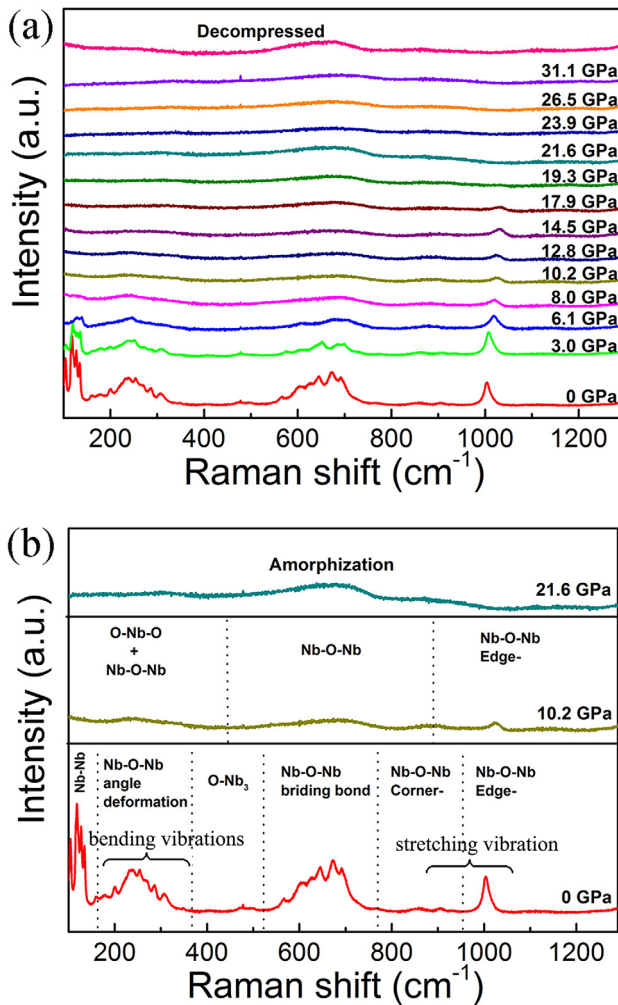


Figure 3. (a) Raman spectra of Nb₂O₅ measured during compression and decompression. (b) Selected Raman spectra of Nb₂O₅ obtained at different pressures, pristine monoclinic Nb₂O₅ phase (bottom), orthorhombic Nb₂O₅ phase at 10.2 GPa (middle), and amorphization phase at 21.6 GPa (top).

a half unit cell dimension. Within a block, NbO₆ units are connected by corner-sharing (sharing one oxygen atom) with each other [33, 47]. The L-Ta₂O₅ phase is built up with an orthorhombic unit cell. The projection on the *bc*-plane and *ab*-plane are shown in figures 5(b) and (c), respectively. Each Nb atom is surrounded by 6 or 7 oxygen atoms, forming distorted octahedra or pentagonal bipyramids. These polyhedra are joined by edge-sharing or corner-sharing.

To unveil and understand the local structural evolution and the amorphization in this system, we carried out high-pressure PDF measurements of Nb₂O₅ up to 25.6 GPa. Figure 6 shows the high-pressure PDF *g(r)* patterns for Nb₂O₅. Several typical peaks for the monoclinic structure in the PDF patterns are indexed at relatively low pressures. The first sharp peak at 1.92 Å corresponds to the Nb–O bond in NbO₆ octahedron, and the second peak at 2.73 Å to the nearest O–O bond. Specifically, the shifts of Nb–O and O–O peaks with pressure are very small, which indicates that these bonds are rigid and difficult to compress. The peaks at 3.31 Å and 3.85 Å may originate from the Nb–Nb1 bonds of the nearest edge-shared

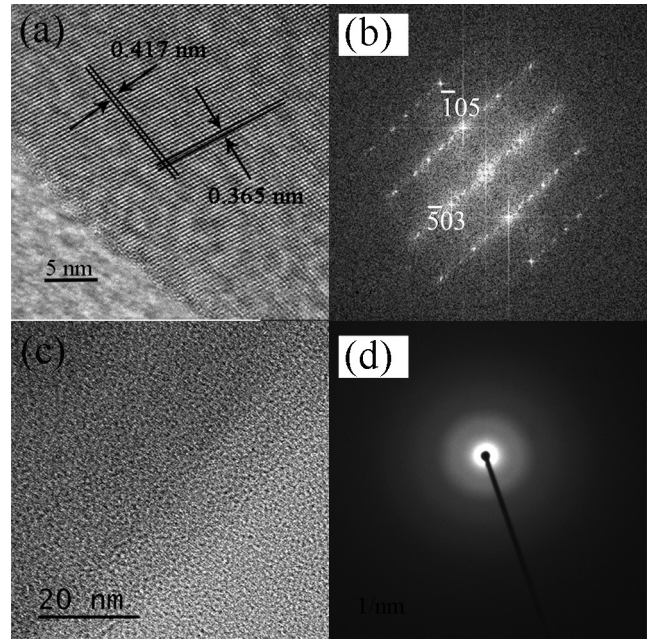


Figure 4. HRTEM images and SAED patterns of the pristine Nb₂O₅ sample (a) and (b), respectively, and the recovered sample from 31.1 GPa (c) and (d), respectively.

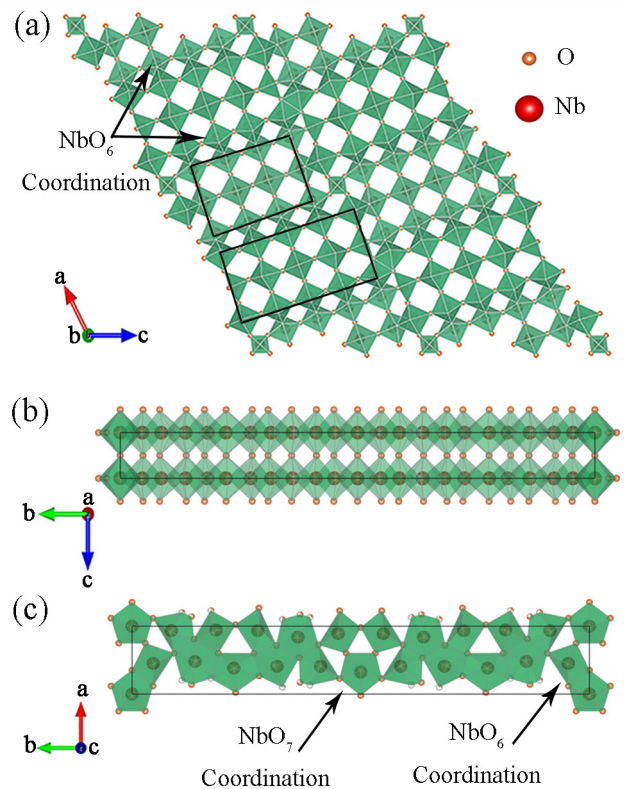


Figure 5. (a) Unit-cell structure of monoclinic Nb₂O₅. Crystal structure of orthorhombic Nb₂O₅, which is built up from edge- and corner-shared NbO₆ octahedra and NbO₇ pentagonal bipyramids: the projection on the *bc*-plane and *ab*-plane are shown in (b) and (c), respectively.

polyhedra and the Nb–Nb₂ bonds of the nearest corner-shared polyhedra, respectively. From 8.5 GPa, we can clearly see that the Nb–Nb₁ peak becomes stronger and the Nb–Nb₂ peak

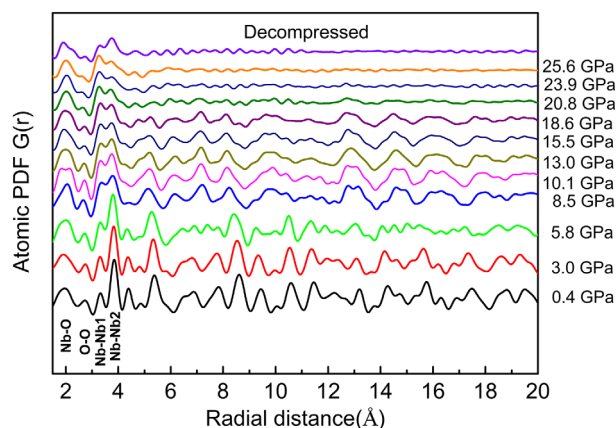


Figure 6. PDFs $g(r)$ for Nb_2O_5 at different pressures.

becomes weaker, indicating that some of the corner-shared NbO_6 octahedra convert into edge-shared NbO_6 octahedra or NbO_7 pentagonal bipyramids accompanied with the transition from the monoclinic phase to the orthorhombic phase. At the amorphization point of 21.4 GPa, peaks corresponding to distances larger than ~ 5 Å start to disappear. Only four peaks at 2.02 Å, 2.67 Å, 3.27 Å and 3.72 Å that represent the bonds within each polyhedra and between the nearest NbO_6 octahedra and NbO_7 pentagonal bipyramids remain. This finding suggests that the local structure, concerning each individual polyhedron and their sharing nature to the nearest polyhedron, are largely preserved in the PIA, but the long-range order of the octahedra or pentagonal bipyramids are broken down in the process. It is clear that the Nb–Nb1 peak becomes stronger than that of Nb–Nb2 above 20.8 GPa. This means increasingly more corner-shared polyhedra transform into edge-shared polyhedra with increasing pressure. It has been found that the corner-shared polyhedra change into edge-shared polyhedra during amorphization and the edge-shared polyhedra with high density are preferred for the amorphous phase under high pressure [12, 16]. Therefore, the corner-shared configuration shows dramatic change under high pressure, i.e. an appreciable number of corner-shared polyhedral would undergo pronounced slip or shifts and even transform into the edge-shared configuration under high pressure. Thus, we suggest that the instability of the corner-shared polyhedra under high pressure plays an important role in the PIA transition in Nb_2O_5 . Remarkably, the peak intensity of Nb–Nb2 is higher than that of Nb–Nb1 in the recovered amorphous sample, which means some edge-shared polyhedra convert back to corner-shared polyhedra under decompression. Obviously, pressure plays an important role in modifying the local structure of the amorphous Nb_2O_5 .

3.5. Optical micrographs and transmission spectra at high pressures

Figure 7(a) shows a few examples of *in situ* high pressure optical micrographs of Nb_2O_5 in a DAC chamber. Under ambient conditions, the material is opaque with a white color. With increasing pressure, we observe a novel phenomenon manifested in the transparency and color, shown in figure S3.

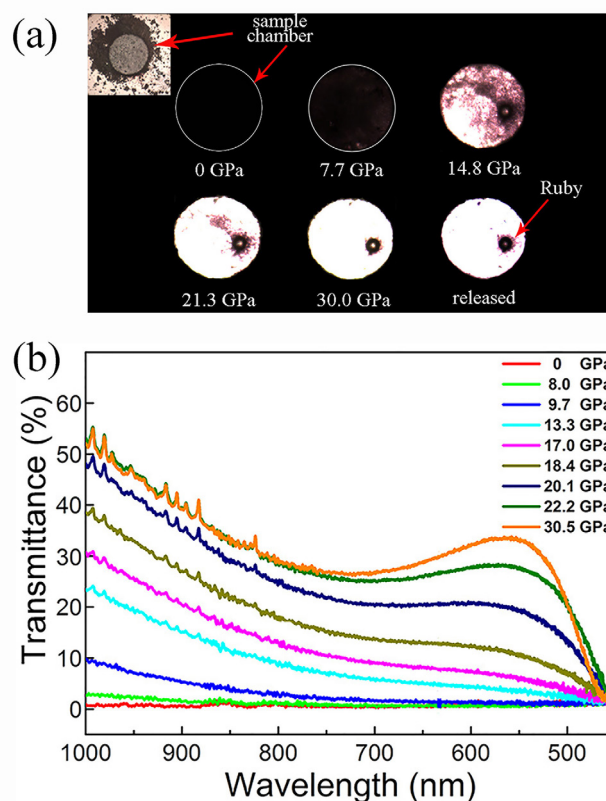


Figure 7. (a) *In situ* high-pressure optical micrographs in a DAC chamber showing the transmittance of Nb_2O_5 ; the inset shows the sample chamber. (b) Transmission spectra of Nb_2O_5 obtained at different pressures.

The sample changes gradually from opaque to partly transparent up to 7.7 GPa, then becomes highly transparent above 21.3 GPa. When the sample is released from 30.0 GPa to ambient pressure, it still shows a high transmittance compared to the initial sample.

We carried out transmission spectroscopy measurements. The optical transmittance of Nb_2O_5 in the wavelength range of 450–1000 nm is shown in figure 7(b). We can see that the sample is initially opaque at ambient pressure (red-line) and the transmittance starts to change in the near infrared region (780–1000 nm) at ~ 8.0 GPa. Particularly, the transmittance increases with increasing pressure to 22.2 GPa, reaching a level of approximately 52% transmission at a wavelength of 1000 nm. When the pressure increases to 30.5 GPa, the optical transmittance is maintained at the same value in the near infrared region, whereas the transmittance in the visible (500–750 nm) increases with increasing pressure. Obviously, the transmittance of Nb_2O_5 can be tuned by pressure. These results provide a new pathway to design materials with tailored properties.

For this change in color, it was observed that after T- Nb_2O_5 reached a pressure of 19.2 GPa, the color of the sample changed from white to black and the sample became amorphous. Serghiou *et al* [19] considered that the color change is probably associated with the formation of reduced niobium oxide defects. For our sample (H- Nb_2O_5), the x-ray absorption near edge structure spectra had no significant changes in

the structure and the absorption Nb K-edges are almost identical, indicating no appreciable change in the oxidation states, experimental results are shown in figure S4. Therefore, we suggest that the pressure-induced reduction of H-Nb₂O₅ does not occur in our case. The pressure-induced reduction is not the reason leading to the PIA in H-Nb₂O₅. Obviously, the PIA mechanism of H-Nb₂O₅ is different from that of T-Nb₂O₅.

4. Conclusions

In summary, the phase transition in H-Nb₂O₅ from the initial monoclinic phase to an orthorhombic phase starts at 5.9 GPa and completes at ~9 GPa. With increasing pressure, the orthorhombic phase transforms into an amorphous form at ~21.4 GPa. The pressure-induced amorphous phase is recoverable at ambient conditions. We suggest that the PIA of Nb₂O₅ is associated with the breakdown of the long-range order of the polyhedra (NbO₆ octahedra and NbO₇ pentagonal bipyramids) and no redox reaction occurred during the amorphization. Interestingly, the *in situ* high-pressure optical micrographs and transmission spectra analysis reveal a dramatic enhancement in the transmittance of the pressure-induced amorphous Nb₂O₅. The results show that PIA could be a useful route for synthesizing new amorphous materials with exceptional properties and unique structural characteristics that possess both amorphous nature lacking long-range order and local structure inherited from parent crystalline phases.

Acknowledgments

This work was financially supported by the NSFC (11374120, 11604116 and 51320105007), National Basic Research Program of China (2011CB808200), Program for Changjiang Scholars and Innovative Research Team in University (No. IRT1132), the visiting scholar project funded by China Scholarship Council, and the Cheung Kong Scholars Programme of China. GS acknowledges the support of DOE-BES/DMSE under Award DE-FG02-99ER45775. HPCAT operations are supported by DOE-NNSA under Award No. DE-NA0001974 with partial instrumentation funding by NSF. The APS is a US Department of Energy (DOE) Office of Science User Facility operated for the DOE Office of Science by ANL under Contract No. DE-AC02-06CH11357.

ORCID iDs

Quanjun Li  <https://orcid.org/0000-0002-4718-4156>
 Changyong Park  <https://orcid.org/0000-0002-3363-5788>
 Bingbing Liu  <https://orcid.org/0000-0002-0152-4469>
 Guoyin Shen  <https://orcid.org/0000-0001-5146-1147>

References

- [1] Mishima O, Calvert L and Whalley E 1984 'Melting ice' I at 77 K and 10 kbar: a new method of making amorphous solids *Nature* **310** 393
- [2] Deb S K, Wilding M, Somayazulu M and McMillan P F 2001 Pressure-induced amorphization and an amorphous–amorphous transition in densified porous silicon *Nature* **414** 528
- [3] Perottoni C and Da Jornada J 1998 Pressure-induced amorphization and negative thermal expansion in ZrW₂O₈ *Science* **280** 886–9
- [4] Sharma S M and Sikka S 1996 Pressure induced amorphization of materials *Prog. Mater. Sci.* **40** 1–77
- [5] Kruger M and Jeanloz R 1990 Memory glass: an amorphous material formed from AlPO₄ *Science* **249** 647–9
- [6] Tse J, Klug D, Ripmeester J, Desgreniers S and Lagarec K 1994 The role of non-deformable units in pressure-induced reversible amorphization of clathrasils *Nature* **369** 724
- [7] Kawai N, Atou T, Ito S, Yubuta K, Kikuchi M, Nakamura K G and Kondo K 2007 Aligned nanocrystalline fragmentation of mullite under shock loading *Adv. Mater.* **19** 2375–8
- [8] Hemley R, Jephcoat A, Mao H K, Ming L and Manghnani M 1988 Pressure-induced amorphization of crystalline silica *Nature* **334** 52
- [9] Gamero-Castano M, Torrents A, Valdevit L and Zheng J-G 2010 Pressure-induced amorphization in silicon caused by the impact of electrosprayed nanodroplets *Phys. Rev. Lett.* **105** 145701
- [10] John S T and Klug D D 1993 Anisotropy in the structure of pressure-induced disordered solids *Phys. Rev. Lett.* **70** 174
- [11] Mukherjee G, Vaidya S and Sugandhi V 2001 Direct observation of amorphous to amorphous apparently first-order phase transition in fused quartz *Phys. Rev. Lett.* **87** 195501
- [12] Li Q, Liu B, Wang L, Li D, Liu R, Zou B, Cui T, Zou G, Meng Y and Mao H 2009 Pressure-induced amorphization and polyamorphism in one-dimensional single-crystal TiO₂ nanomaterials *J. Phys. Chem. Lett.* **1** 309–14
- [13] Swamy V, Kuznetsov A, Dubrovinsky L S, McMillan P F, Prakapenka V B, Shen G and Muddle B C 2006 Size-dependent pressure-induced amorphization in nanoscale TiO₂ *Phys. Rev. Lett.* **96** 135702
- [14] Wang L, Yang W, Ding Y, Ren Y, Xiao S, Liu B, Sinogeikin S V, Meng Y, Gosztoła D J and Shen G 2010 Size-dependent amorphization of nanoscale Y₂O₃ at high pressure *Phys. Rev. Lett.* **105** 095701
- [15] Arora A, Sato T, Okada T and Yagi T 2012 High-pressure amorphous phase of vanadium pentoxide *Phys. Rev. B* **85** 094113
- [16] Lü X, Hu Q, Yang W, Bai L, Sheng H, Wang L, Huang F, Wen J, Miller D J and Zhao Y 2013 Pressure-induced amorphization in single-crystal Ta₂O₅ nanowires: a kinetic mechanism and improved electrical conductivity *J. Am. Chem. Soc.* **135** 13947–53
- [17] Kikuchi M, Kusaba K, Bannai E, Fukuoka K, Syono Y and Hiraga K 1985 Observation of shock-induced phases of Nb₂O₅ single crystal under high-resolution electron microscopy *Japan. J. Appl. Phys.* **24** 1600
- [18] Kikuchi M, Kusaba K, Fukuoka K and Syono Y 1986 Formation of rutile-type Nb_{0.94}O₂ by shock reduction of Nb₂O₅ *J. Solid State Chem.* **63** 386–90
- [19] Serghiu G C, Winters R R and Hammack W S 1992 Pressure-induced amorphization and reduction of T-Nb₂O₅ *Phys. Rev. Lett.* **68** 3311
- [20] Tse J S, Klug D D and Lu Z 1994 X-ray-photoelectron and x-ray-photoabsorption study of pressure-amorphized T-Nb₂O₅ *Phys. Rev. B* **49** 9180–1
- [21] Lü X, Wang Y, Stoumpos C C, Hu Q, Guo X, Chen H, Yang L, Smith J S, Yang W and Zhao Y 2016 Enhanced structural stability and photo responsiveness of CH₃NH₃SnI₃ perovskite via pressure-induced amorphization and recrystallization *Adv. Mater.* **28** 8663–8

- [22] Wang Y, Lü X, Yang W, Wen T, Yang L, Ren X, Wang L, Lin Z and Zhao Y 2015 Pressure-induced phase transformation, reversible amorphization, and anomalous visible light response in organolead bromide perovskite *J. Am. Chem. Soc.* **137** 11144–9
- [23] Szafranski M and Katrusiak A 2016 Mechanism of pressure-induced phase transitions, amorphization, and absorption-edge shift in photovoltaic methylammonium lead iodide *J. Phys. Chem. Lett.* **7** 3458–66
- [24] Santamaria-Perez D, Thomson A, Segura A, Pellicer-Torres J, Manjon F J, Corà F, McColl K, Wilson M, Dobson D and McMillan P F 2016 Metastable structural transformations and pressure-induced amorphization in natural (Mg, Fe)₂SiO₄ olivine under static compression: a Raman spectroscopic study *Am. Mineral.* **101** 1642–50
- [25] Goel P, Gupta M, Mittal R, Rols S, Achary S, Tyagi A and Chaplot S 2015 Inelastic neutron scattering studies of phonon spectra, and simulations of pressure-induced amorphization in tungstates AWO₄ (A = Ba, Sr, Ca, and Pb) *Phys. Rev. B* **91** 094304
- [26] Soares M, Leite S, Nico C, Peres M, Fernandes A, Graça M, Matos M, Monteiro R, Monteiro T and Costa F 2011 Effect of processing method on physical properties of Nb₂O₅ *J. Eur. Ceram. Soc.* **31** 501–6
- [27] Pozdeev Y 1998 Reliability comparison of tantalum and niobium solid electrolytic capacitors *Qual. Reliab. Eng. Int.* **14** 79–82
- [28] He J, Hu Y, Wang Z, Lu W, Yang S, Wu G, Wang Y, Wang S, Gu H and Wang J 2014 Hydrothermal growth and optical properties of Nb₂O₅ nanorod arrays *J. Mater. Chem. C* **2** 8185–90
- [29] Griffith K J, Forse A C, Griffin J M and Grey C P 2016 High-rate intercalation without nanostructuring in metastable Nb₂O₅ bronze phases *J. Am. Chem. Soc.* **138** 8888–99
- [30] Chen D, Wang J-H, Chou T-F, Zhao B, El-Sayed M A and Liu M 2017 Unraveling the nature of anomalously fast energy storage in T-Nb₂O₅ *J. Am. Chem. Soc.* **139** 7071–81
- [31] Nico C, Monteiro T and Graça M 2016 Niobium oxides and niobates physical properties: review and prospects *Prog. Mater. Sci.* **80** 1–37
- [32] Zhao Y, Zhou X, Ye L and Chi Edman Tsang S 2012 Nanostructured Nb₂O₅ catalysts *Nano Rev.* **3** 17631
- [33] Valencia-Balvín C, Pérez-Walton S, Dalpian G and Osorio-Guillén J 2014 First-principles equation of state and phase stability of niobium pentoxide *Comput. Mater. Sci.* **81** 133–40
- [34] Klotz S, Chervin J-C, Munsch P and Le Marchand G 2009 Hydrostatic limits of 11 pressure transmitting media *J. Phys. D: Appl. Phys.* **42** 075413
- [35] Sysssen K 2008 Ruby under pressure *High Press. Res.* **28** 75–126
- [36] Toby B H 2001 EXPGUI, a graphical user interface for GSAS *J. Appl. Crystallogr.* **34** 210–3
- [37] Qiu X, Thompson J W and Billinge S J 2004 PDFgetX2: a GUI-driven program to obtain the pair distribution function from x-ray powder diffraction data *J. Appl. Crystallogr.* **37** 678
- [38] Zibrov I, Filonenko V, Werner P-E, Marinder B-O and Sundberg M 1998 A new high-pressure modification of Nb₂O₅ *J. Solid State Chem.* **141** 205–11
- [39] Tamura S 1972 High-pressure phase research on Nb₂O₅ *J. Mater. Sci.* **7** 298–302
- [40] Filonenko V and Zibrov I 2001 High-pressure phase transitions of M₂O₅ (M = V, Nb, Ta) and thermal stability of new polymorphs *Inorg. Mater.* **37** 953–9
- [41] Aleshina L and Loginova S 2002 Rietveld analysis of x-ray diffraction pattern from β-Ta₂O₅ oxide *Crystallogr. Rep.* **47** 415–9
- [42] Askeljung C, Marinder B-O and Sundberg M 2003 Effect of heat treatment on the structure of L-Ta₂O₅: a study by XRPD and HRTEM methods *J. Solid State Chem.* **176** 250–8
- [43] Marinder B-O 2001 Moser's C-line, the apparent multiplicity *m'* and modules in descriptions of L-Ta₂O₅ and related structures *J. Solid State Chem.* **160** 62–8
- [44] Dhawan S, Dhawan T and Vedeshwar A G 2014 Residual stress induced crystalline to amorphous phase transformation in Nb₂O₅ quantum dots *J. Appl. Phys.* **116** 043503
- [45] Li Y and Gao L 2003 Synthesis and characterization of nanocrystalline niobium nitride powders *J. Am. Ceram. Soc.* **86** 1205–7
- [46] Ikeya T and Senna M 1988 Change in the structure of niobium pentoxide due to mechanical and thermal treatments *J. Non-Cryst. Solids* **105** 243–50
- [47] Balachandran U and Eror N G 1982 Raman spectrum of the high temperature form of Nb₂O₅ *J. Mater. Sci. Lett.* **1** 374–6
- [48] Dobal P, Katiyar R, Jiang Y, Guo R and Bhalla A 2000 Raman scattering study of a phase transition in tantalum pentoxide *J. Raman Spectrosc.* **31** 1061–5
- [49] Joseph C, Bourson P and Fontana M 2012 Amorphous to crystalline transformation in Ta₂O₅ studied by Raman spectroscopy *J. Raman Spectrosc.* **43** 1146–50
- [50] Shuker R and Gammon R 1970 Raman-scattering selection-rule breaking and the density of states in amorphous materials *Phys. Rev. Lett.* **25** 222–5